OPEN

Citation: Cell Death and Disease (2014) 5, e1368; doi:10.1038/cddis.2014.320

www.nature.com/cddis

The LRRK2 inhibitor GSK2578215A induces protective autophagy in SH-SY5Y cells: involvement of Drp-1-mediated mitochondrial fission and mitochondrial-derived ROS signaling

S Saez-Atienzar[1,2,3], L Bonet-Ponce[2], JR Blesa[2], FJ Romero[2], MP Murphy[4], J Jordan[1] and MF Galindo*[,3]

Mutations in the leucine-rich repeat kinase 2 (*LRRK2*) gene have been associated with Parkinson's disease, and its inhibition opens potential new therapeutic options. Among the drug inhibitors of both wild-type and mutant LRRK2 forms is the 2-arylmethyloxy-5-subtitutent-*N*-arylbenzamide GSK257815A. Using the well-established dopaminergic cell culture model SH-SY5Y, we have investigated the effects of GSK2578215A on crucial neurodegenerative features such as mitochondrial dynamics and autophagy. GSK2578215A induces mitochondrial fragmentation of an early step preceding autophagy. This increase in autophagosome results from inhibition of fusion rather than increases in synthesis. The observed effects were shared with LRRK2-IN-1, a well-described, structurally distinct kinase inhibitor compound or when knocking down LRRK2 expression using siRNA. Studies using the drug mitochondrial division inhibitor 1 indicated that translocation of the dynamin-related protein-1 has a relevant role in this process. In addition, autophagic inhibitors revealed the participation of autophagy as a cytoprotective response by removing damaged mitochondria. GSK2578215A induced oxidative stress as evidenced by the accumulation of 4-hydroxy-2-nonenal in SH-SY5Y cells. The mitochondrial-targeted reactive oxygen species scavenger MitoQ positioned these species as second messengers between mitochondrial morphologic alterations and autophagy. Altogether, our results demonstrated the relevance of LRRK2 in mitochondrial-activated pathways mediating in autophagy and cell fate, crucial features in neurodegenerative diseases.
Cell Death and Disease (2014) **5,** e1368; doi:10.1038/cddis.2014.320; published online 14 August 2014

Nowadays, Parkinson's disease (PD) constitutes the main motor disorder and the second neurodegenerative disease after Alzheimer's disease. Etiology of PD remains unknown, but both environmental and genetic factors have been implicated. Among the genes associated with PD is the leucine-rich repeat kinase 2 (LRRK2, *PARK8*, OMIM 607060) encoding gene encoded by PARK8. Indeed, LRRK2 mutations have been described in a substantial number of idiopathic late-onset PD patients without a known family history of the disease.[1–3]

The physiologic function remains unknown. It localizes in the cytosol as well as in specific membrane subdomains, including mitochondria, autophagosomes and autolysosomes,[4] and interacts with a whole array of proteins, including both α- and β-tubulin,[5,6] tau,[7] α-synuclein[8] and F-actin.[9] LRRK2 gene mutations, including the most common G2019S,[3] are associated with increases in toxic putative kinase activity.[1,10] LRRK2 overexpression is toxic to cultured cells,[11,12] and LRRK2 loss did not cause neurodegenerative changes (for a review see Tong and Shen[13]). However, LRRK2 transgenic mice lack obvious PD-like behavioral phenotypes.[14] LRRK2-associated PD patients show degeneration of dopaminergic neurons in the substantia nigra.[15] Data from our own group and others have associated mitochondrial apoptotical pathways with PD,[16–18] and, in this context, LRRK2 mutant-mediated toxicity could be due to mitochondria-dependent apoptosis.[19] There is considerable evidence for impaired mitochondrial function and morphology in both early-onset, autosomal recessive inherited PD and late-onset sporadic PD.

Mitochondrial dynamics include several mechanisms, such as fission, fusion and mitophagy.[20,21] Altered fission/fusion dynamics might be a common pathogenic pathway of neurodegenerative diseases. It is well documented that mitochondrial dynamics constitute a relevant issue in some experimental neurodegenerative models.[20,22–25] Mitochondrial dynamics is tightly regulated by cellular pathways including those participated by the dynamin-related protein-1 (Drp1). Drp1 mostly locates in the cytoplasm, but is stimulated after fission stimuli to migrate to the mitochondria. Once there, Drp1 forms ring-like structures, which wrap around the scission site to constrict the mitochondrial

[1]Grupo de Neurofarmacología, Dpto. Ciencias Médicas, Facultad de Medicina de Albacete, Universidad de Castilla-La Mancha, IDINE, Albacete, Spain; [2]Facultad de Medicina y Odontología, Universidad Católica de Valencia 'San Vicente Mártir' Valencia, Valencia, Spain; [3]Unidad de Neuropsicofarmacología Traslacional, Complejo Hospitalario Universitario de Albacete, Albacete, Spain and [4]Mitochondrial Biology Unit, Wellcome Trust/MRC Building, Hills Road, Cambridge, UK
*Corresponding author: MF Galindo, Unidad de Neurofarmacología Traslacional, Complejo Hospitalario Universitario de Albacete, C/ Hermanos Falcó 37, 02006 Albacete, Spain. Tel: +34 967 597477; Fax: +34-967 597173; E-mail: mgalindoa@sescam.jccm.es
Abbreviations: CHX, cycloheximide; Drp1, dynamin-related protein 1; GFP, green fluorescent protein; 4-HNE, hydroxyalkenal 4-hydroxy-2-nonenal; LC3, microtubule-associated protein 1A/1B-light chain 3; LRRK2, leucine-rich repeat kinase 2; mdivi-1, mitochondrial division inhibitor-1; PD, Parkinson's disease; RFP, red fluorescent protein; ROS, reactive oxygen species
Received 18.12.13; revised 09.6.14; accepted 13.6.14; Edited by GM Fimia

membrane resulting in mitochondrial fission.[26,27] Interestingly, a functional interaction between PD-associated LRRK2 and members of the dynamin GTPase superfamily has been described.[28]

Macroautophagy (hereafter referred to as autophagy) is an active cellular response, which functions in the intracellular degradation system of cellular debris such as damaged organelles. Whether autophagy promotes cell death or enhances survival is still controversial.[29,30] It requires the formation of autophagosomes where cellular content is to be degraded by the action of lysosomal enzymatic content. Autophagosome formation is regulated by an orderly action of >30 autophagy-related (Atg) proteins. Among them is the microtubule-associated protein 1A/1B-light chain 3 (LC3), a homolog of Apg8p, which is essential for autophagy in yeast and is associated with autophagosome membranes.[31] Interestingly, these vesicles are mostly highly mobile in the cytoplasm.[32] Wild-type and mutant LRRK2 expression has been related to autophagy.[4,33–36] Reactive oxygen species (ROS) function as relevant second messengers after several stimuli, including mitochondrial disruption. Exacerbated ROS increases might result in overactivation of antioxidant systems and yield harmful oxidative stress. Among oxidative stress hallmarks is the accumulation of α,β-unsaturated hydroxyalkenal 4-hydroxy-2-nonenal (4-HNE), whose accumulation has been reported in PD post-mortem patient brains,[37,38] thus giving a significant relevance to ROS in the pathogenesis of PD.

All these results indicate LRRK2 as a promising pharmacologic target in PD treatment.[39] Several LRRK2 inhibitor drugs have been synthetized, such as the potent and highly selective 2-arylmethyloxy-5-substitutent-*N*-arylbenzamide (GSK2578215A). GSK2578215A exhibits biochemical IC_{50}s of 10.9 nM against wild-type LRRK2, and possesses a high ratio of brain to plasma distribution.[40] This study provides key insights into the mechanisms downstream of LRRK2 inhibition, and spreads light onto an underexplored, yet potentially tractable therapeutic target for treating LRRK2-associated PD. We demonstrate how inhibition of this kinase results in the activation of cellular death pathways such as the mitochondrial fission machinery, and how cells reply by activating a protective autophagic response. Our results show the presence of oxidative stress hallmarks, thus pointing to a key function for ROS, placed downstream of mitochondrial fission.

Results

We used GSK2578215A at a concentration of 1 nM to study the effects of LRRK2 inhibition on SH-SY5Y after 12 h of treatment. In the first set of experiments, we studied if administration of GSK2578215A at this concentration results in the inhibition of LRRK2 kinase activity. We assayed the effects on F-actin distribution.[41,42] To this end, we transiently overexpressed LifeAct-TagGFP2 to localize intracellular F-actin distribution in SH-SY5Y cells. F-actin presents a homogeneous distribution in non-treated cells (Supplementary Figure 1a), whereas in 1 nM GSK2578215A-challenged cell cultures, the F-actin distribution was altered from a rather homogeneous to a more peripheral distribution (Supplementary Figure 1b). Next, we determined the levels of LRRK2 phosphorylation on residue S935 and total LRRK2 protein levels. Addition of GSK2578215A led to a decrease of S935 LRRK2 phosphorylation but not of total LRRK2 protein levels (Supplementary Figure 1b). Taken together, these results show that 1 nM GSK2578215A-induced LRRK2 inhibition results in the disruption of downstream pathways described for LRRK2.[41,42]

GSK2578215A induces autophagy. We ascertained the participation of autophagy by transiently transfecting SH-SY5Y cell cultures with the GFP-LC3 plasmid, which allows monitoring of the formation of autophagosomes. Briefly, SH-SY5Y cells seeded on IDIBI-coated dishes were transfected with GFP-LC3 plasmid. One day after transfection, cells were treated with GSK2578215A (1 nM) and 12 h later imaged in a confocal microscopy (Figure 1a). In untreated control cell cultures, independently of the time point assayed, we detected about 10% of autophagic cells (Figure 1b). GSK2578215A treatments required 9 h to start inducing significant increases in autophagic cell percentage (Figure 1b). Next, we assayed the levels of endogenous LC3 and p62 in cell cultures challenged with GSK2578215A. Figure 1c shows representative immunoblots, demonstrating that the levels of both proteins increased in a time-dependent manner upon the addition of 1 nM GSK2578215A. Interestingly, the increase of p62 levels was abrogated by adding cycloheximide (CHX), an experimental tool to block protein synthesis (Supplementary Figure 1C).

To verify if the above-described GSK2578215A-induced effects can be generalized to other LRRK2 inhibitors, two different approaches were used. First, cell cultures were challenged with LRRK2-IN-1 (5 μM, 12 h), a well-established LRRK2 inhibitor. LRRK2-IN-1 induced similar effects as GSK2578215A on autophagy (Figure 1d). Second, SH-SY5Y cells were co-transfected with siRNA to knock down LRRK2 expression and GFP-LC3 plasmid, leading to an increase in the percentage of autophagic cells (Figure 1d). Taken together, these data show that the effect of GSK2578215A was an LRRK2-dependent phenomenon and not an off-target effect of the inhibitor.

GSK2578215A impairs autophagosome/lysosome fusion. GSK2578215A treatments induced an increase in the number of autophagosomes per cell (Figure 1e). The accumulation of autophagosomes may be due to an increase of autophagosome synthesis, disruption of autophagosome/lysosome fusion, or both. We used the lysosome inhibitor chloroquine (CQ), which clamps the degradation, to study the effect of GSK2578215A on autophagy flux (Figure 1a). After 24 h of GFP-LC3 transfections, cells were treated with 50 μM CQ, and then challenged with GSK2578215A. Using confocal microscopy, 12 h later we determined the number of GFP-LC3 punctuates within each cell. Cells treated with CQ alone presented an increase in the number of GFP-LC3 dots (Figure 1e).

In addition, the number of dots in the cells challenged with both CQ and GSK2578215A was also increased (Figure 1e). Taken together, based on the changes in the number of GFP-LC3 dots, these data indicate that there was an apparent increase in autophagosome synthesis.

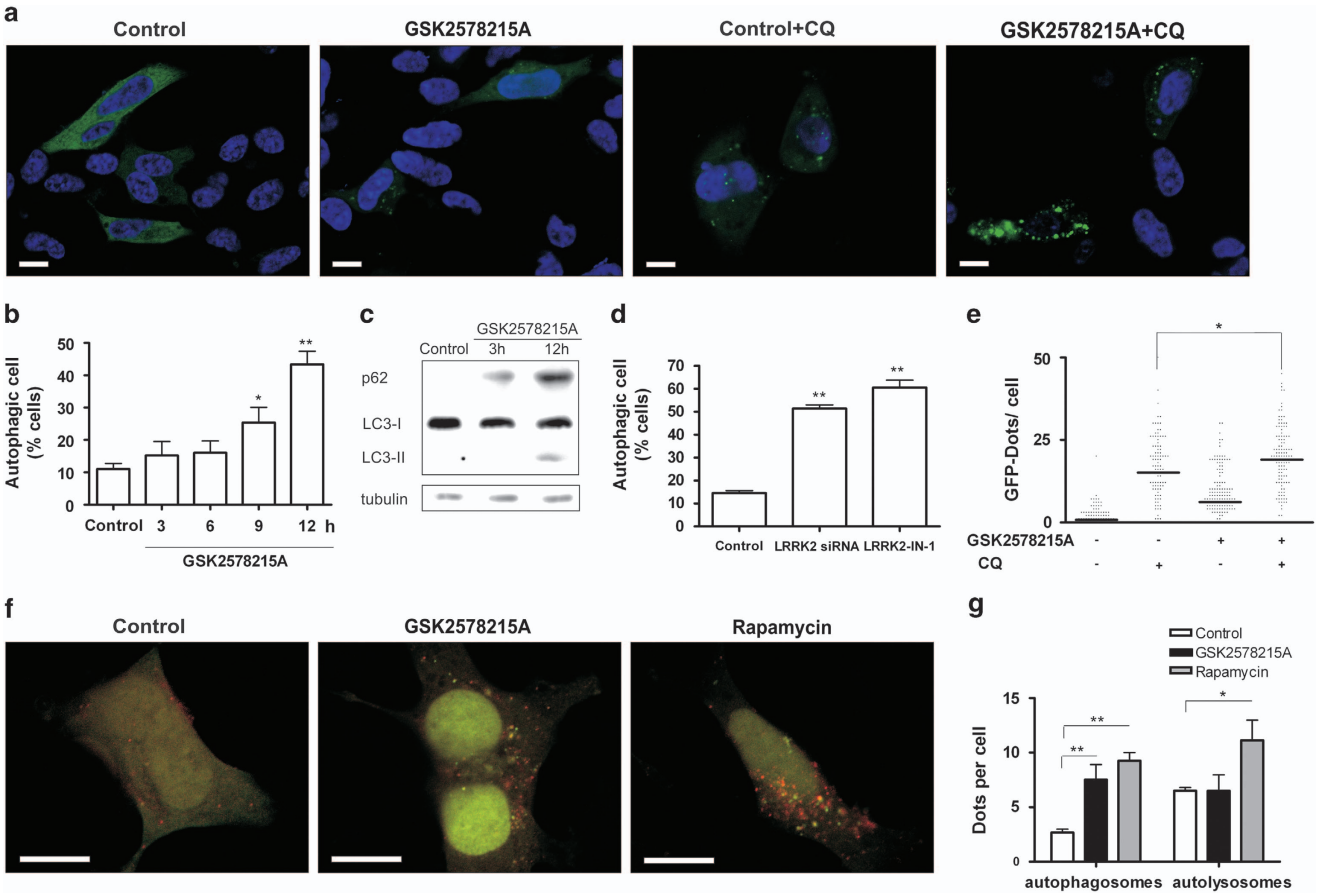

Figure 1 GSK257815A activates autophagy in SH-SY5Y cells. (**a**) Confocal images of SH-SY5Y cells transfected with GFP-LC3 vector. Twenty-four hours after transfection, cells were treated with 1 nM GSK2578215A for 12 h in the presence or absence of CQ (50 μM). Untreated control cells showed diffuse cytosolic GFP-LC3 distribution, whereas those treated with GSK2578215A, CQ, or both presented increased numbers of GFP-LC3 dots per cell. (**b**) Histogram showing the percentage of autophagic cells (cells with more than six GFP-LC3 dots) at 3, 6, 9 and 12 h after 1 nM GSK2578215A addition. (**c**) Western blot analysis of p62 and LC3 protein levels using lysates of SH-SY5Y cells, which were treated or not with 1 nM GSK257815A for 3 or 12 h. Tubulin was used as a loading control. All data are representative of three independent experiments. (**d**) Histogram representing the effects of LRRK2 knockdown (siRNA) and LRRK2-IN-1 (5 μM, 12 h) in SH-SY5Y cells on autophagy. (**e**) Dot graph representing the number of GFP-LC3 dots per cell, treated or not with GSK2578215A in the absence or presence of CQ. Autophagic flux values for synthesis calculated as detailed in the Materials and Methods section. (**f**) Confocal microscopy pictures of SH-SY5Y cells transfected with mRFP-GFP-LC3. Twenty-four hours after transfection, cells were treated with 1 nM GSK2578215A. (**g**) Quantification of autophagosomes (yellow dots) and autolysosomes (red dots). Rapamycin (10 nM) was used as a positive control. Hoechst staining was used to show the chromatin state. Data shown in histograms are the means ± S.E.M. of at least three independent experiments, each performed in triplicate. Statistical significance was determined by a two-tailed Student's *t*-test: $^{*}P<0.05$ and $^{**}P<0.01$. Scale bars, 10 μm

For further analysis of autophagosome maturation, we took advantage of the mRFP-GFP-LC3 tandem reporter.[43] Within lysosomes, GFP-LC3 fluorescence is quenched because of the sensitivity of GFP to acidic environments, whereas mRFP-LC3 fluorescence is more stable upon acidification. Thus, autophagosomes with a physiologic pH will show both red and green fluorescence, whereas the latter is lost in autolysosomes with an acidic pH. GSK2578215A treatment resulted in an increase in the number of autophagosomes (yellow dots) and a similar number of autolysosomes (red dots). Rapamycin, in a concentration of 10 nM, was used as a positive control of autophagy (Figures 1f and g). We conclude from these data that GSK2578215A impairs the autophagy flux by altering autophagosome–lysosome fusion.

GSK2578215A induces Drp-1-mediated mitochondrial fission. Mitochondrial morphology was examined in cell cultures that were transfected with pDsRed2-mito plasmid to express the mitochondrial protein DsRed2. Control cell cultures presented long mitochondria forming a net with a homogeneous intracellular distribution (Figure 2a). By 6 h, but not 3 h after 1 nM GSK2578215A addition, mitochondrial morphology alterations were evident. Mitochondrial filament size had decreased and the mitochondrial net was disrupted (Figure 2b). Using Hoechst staining, it was observed that cells with fragmented mitochondria failed to show alterations in the chromatin state. This indicates that this organelle alteration was not a result of cell death (Figure 2b). The quantification of this morphologic alteration, as percentage of cells with fragmented mitochondria, confirmed that it was a time-dependent effect, as a 6-h interval was necessary to observe this effect (Figure 2d). Consistent with an LRRK2-dependent phenomenon and not an off-target effect of the inhibitor, both LRRK2-IN-1 (5 μM, 12 h) and knockdown of LRRK2 expression induced mitochondrial fission (Figure 2e).

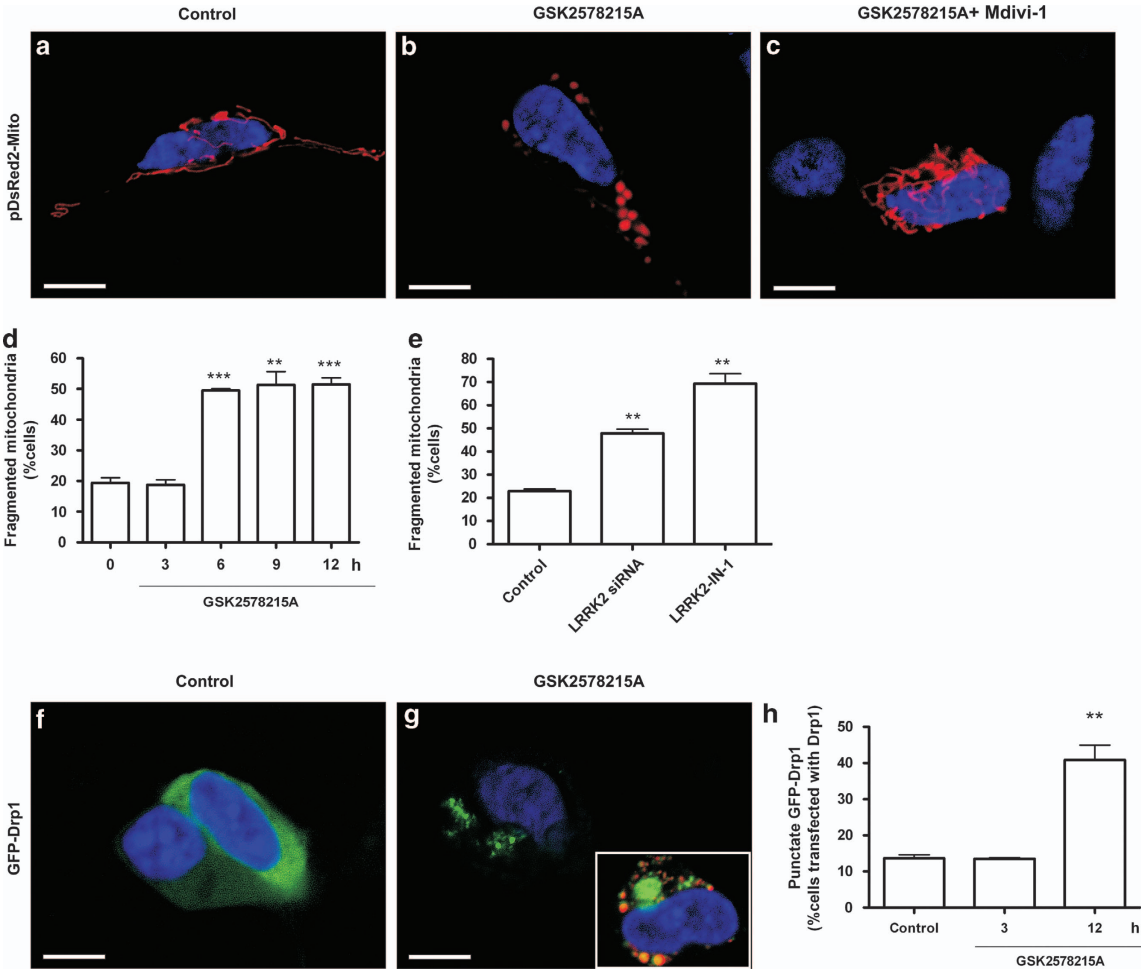

Figure 2 GSK2578215A induces Drp1-mediated mitochondrial fission. (**a**–**c**) Representative confocal images of SH-SY5Y cells transfected with the pDsRed2-mito vector. Twenty-four hours after transfection, cells were treated or not (**a**) with 1 nM GSK2578215A for 12 h (**b**) and cotreated with 10 μM mdivi-1 (**c**). (**d**) Histogram representing the percentage of cells with fragmented mitochondria at the times indicated. (**e**) Histogram representing the effects of LRRK2-IN-1 (5 μM, 12h) and LRRK2 knockdown in SH-SY5Y cells on mitochondria morphology. (**f–h**) GSK2578215A induces mitochondrial Drp1 translocation. Representative confocal images of SH-SY5Y cells transfected for 24 h with GFP-Drp1 in non-treated cells (**f**) or cells incubated with 1 nM GSK2578215A for 12 h (**g**). Inset illustrates colocalization of GFP-Drp1 and fragmented mitochondria. (**h**) After 3 and 12 h of treatment, the number of cells with punctate GFP-Drp1 distribution was counted and expressed as the percentage of cells expressing GFP-Drp1. Scale bar, 10 μM. Data shown are the mean ± S.E.M. of at least three independent experiments, each performed in triplicate. Statistical significance was determined by a two-tailed Student's *t*-test: $^{***}P<0.001$. Scale bar, 10 μM

Next, we studied whether GSK2578215A activates Drp1 translocation from the cytosol to mitochondria by examining the location of a GFP-tagged Drp1 (GFP-Drp1). As shown in Figure 2f, untreated cultures presented a homogeneous cytosolic distribution of GFP-Drp1. However, we detected an increase in the percentage of cells with a punctuated GFP-Drp1 distribution after 6 h (Figures 2g and h), and the punctated protein colocalized with fragmented mitochondria (Figure 2g, inset). Furthermore, using the chemical inhibitor of Drp-1 activity mitochondrial division inhibitor-1 (mdivi-1),[44] participation of Drp-1 in GSK2578215A-induced mitochondrial fission was confirmed (Figure 2c).

GSK2578215A induces mitophagy. Next, the plausible relationship between mitochondrial fission and autophagy was studied. To this end, SH-SY5Y cells were co-transfected with pDsRed2-mito and GFP-LC3 plasmids, and analyzed the localization of the corresponding expressed proteins by confocal microscopy (Figures 3a–f). Twenty-four hours after GSK2578215A addition, we frequently observed colocalization of fragmented mitochondrial with autophagosomes (Figure 3f). Consistently, the distance between mitochondria and autophagosome decreased in a time-dependent manner (Figure 3g). Consistent with the role of Drp-1, mdivi-1 decreased the percentage of autophagic cells in GSK2578215A-challenged cultures (Figure 3h).

Role of mitochondrial-derived ROS. To gain insight into the cellular mechanism activated by GSK2578215A, we investigated the relevance of ROS by analyzing 4-HNE intracellular levels. Using immunofluorostaining we detected that GSK2578215A markedly promoted this marker of lipid oxidative damage in SH-SY5Y cells (Figures 4a–c). A quantitative analysis revealed that 1 nM GSK2578215A induced significant accumulation of 4-HNE after 12 h of treatment (Figure 4c).

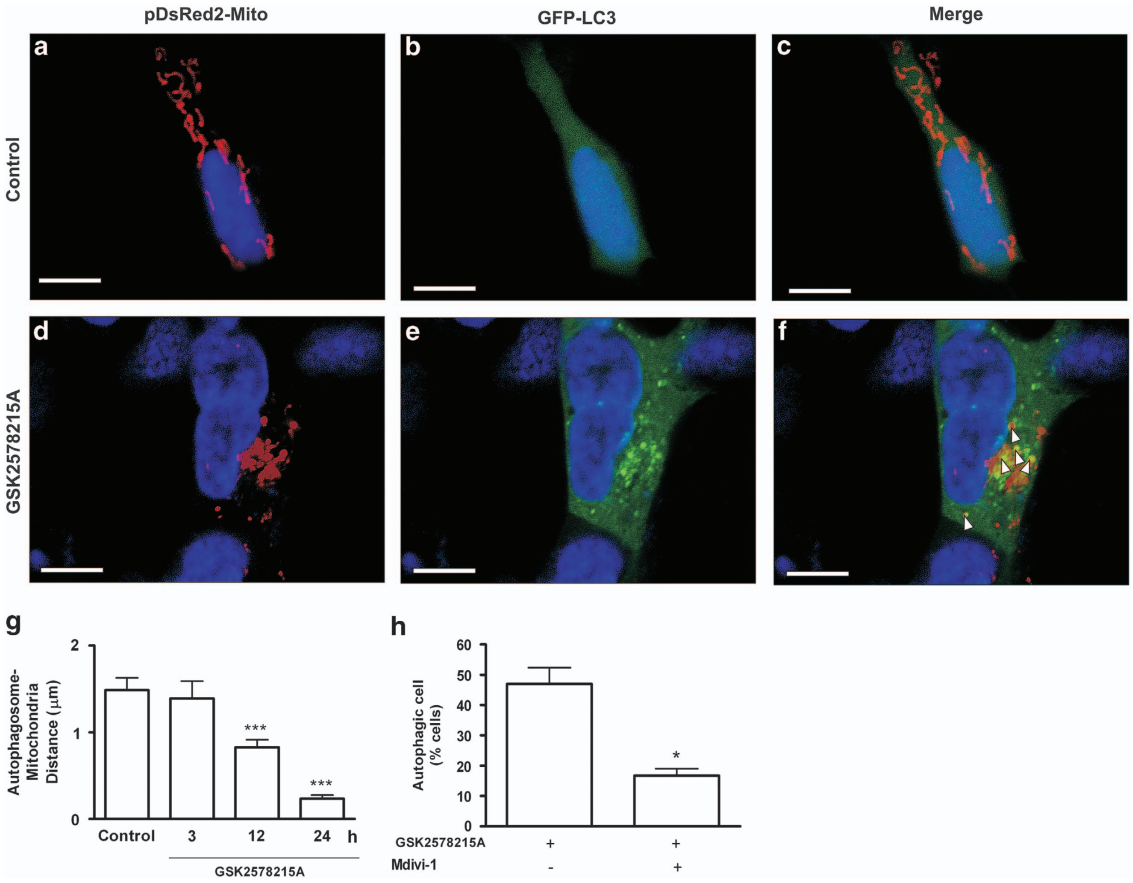

Figure 3 GSK2578215A induces mitophagy. (**a–g**) SH-SY5Y cells were co-transfected with pDsRed2-mito and GFP-LC3 plasmids and 24 h later treated with GSK2578215A. Confocal microscopy pictures showing the mitochondrial morphology (**a** and **d**) and the localization of GFP-LC3 vesicles (**b** and **e**). In (**f**), arrows indicate the colocalization of both proteins. (**g**) Bar diagram representing the distance between mitochondria and autophagosomes in treated and untreated control cells at the times indicated. (**h**) The inhibition of mitochondrial fission by mdivi-1 blocks GSK2578215A-induced autophagy in SH-SY5Y cells. At 24 h after transfection with GFP-LC3, SH-SY5Y cells were treated with 1 nM GSK2578215A in the presence or absence of 10 μM mdivi-1, and 12 h later, the percentage of autophagic cells was determined. Nuclei were stained with Hoechst. Data shown in the bar graph are the mean ± S.E.M. of at least three independent experiments, each performed in triplicate. Statistical significance was determined by a two-tailed Student's *t*-test: $^{*}P<0.05$ and $^{***}P<0.001$. Scale bar, 10 μm

To ascertain the role of mitochondrial-derived ROS, we used the mitochondria-targeted antioxidant MitoQ. As shown in Figure 4d, 50 nM MitoQ decreased the percentage of autophagic cells after 12 h of treatment. However, MitoQ failed to prevent GSK2578215A-induced mitochondrial fragmentation (Figure 4e). These results support the notion that oxidative stress-derived lipid peroxidation product formation takes place downstream of mitochondrial disruption.

Autophagy acts as a cytoprotective response against GSK2578215A. There is controversy about the role of autophagy on cell fate. We thus characterized the effect of GSK2578215A on SH-SY5Y cell viability. As illustrated in Figure 5, 1 nM GSK2578215A induced cytotoxicity of cell cultures. By using Hoechst 33342, we noted an increase in the percentage of cells with apoptotical chromatin hallmarks, such as condensation or fragmentation (Figures 5a and b). In addition, by using the TdT-mediated dUTP-biotin nick-end labeling method (TUNEL) technique, we evidenced the presence of endonucleolytic cleavage of chromatin in cultures that were treated for 12 h (Figure 5d), but not in control cultures (Figure 5c). Consistently, percentages of cells showing death-like morphology (see Materials and Methods) increased with exposure time to GSK2578215A, reaching significant differences by 12 h after addition (Figure 5e). Interestingly, cell cultures challenged with LRRK2-IN-1 also presented a similar increase in cell death percentage (Figure 2f).

Finally, we used two autophagic inhibitor drugs, 3-methyladenine (3-MA, 5 mM) or CQ (50 μM), at early or late steps, respectively. Treatment with either of these drugs showed no effect on SH-SY5Y cell viability, but both drugs enhanced GSK2578215A-induced cell death (Figure 5g). In cell cultures cotreated with GSK2578215A and either 3-MA or CQ, cell death percentages increased by 98 ± 2.68% ($P<0.05$; $n=3$) and 73 ± 2.22% ($P<0.05$; $n=3$), respectively, after 12 h after GSK2578215A addition.

Discussion

We herein dissected the mechanisms underlying LRRK2 inhibition by GSK2578215A on the neuroblastoma dopaminergic cell line SH-SY5Y. We used GSK2578215A at 1 nM, which induced LRRK2 inhibition, resulting in the disruption of downstream pathways.[41,42] GSK2578215A activates the

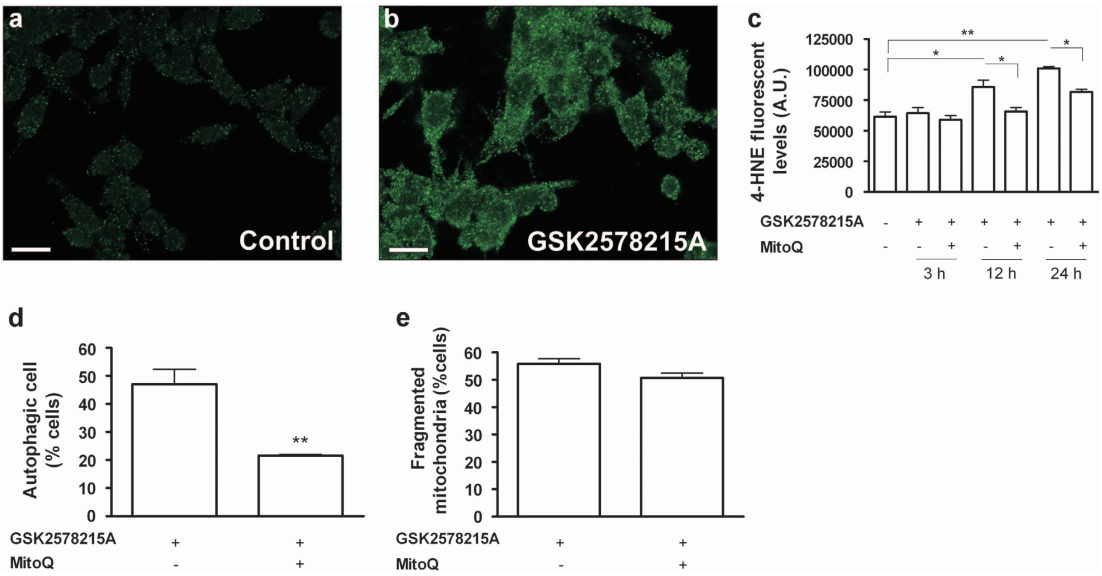

Figure 4 Role of ROS in GSK2578215A-induced effects. (**a–c**) GSK2578215A increased the intracellular 4-HNE levels in a time-dependent manner. Representative confocal images of 4-HNE immunofluorostaining (green) in SH-SY5Y cells at $t = 0$ (**a**) and after 24 h (**b**) of 1 nM GSK2578215A treatment. Scale bars, 20 μm. (**c**) Bar graph illustrating the 4-HNE fluorescence levels from confocal images expressed as arbitrary units (a.u.). (**d** and **e**) Effect of MitoQ on GSK257815A-induced alterations in SH-SY5Y cells. Cells were transfected with either pDsRed2-mito or GFP-LC3 plasmid, and 24 h later pretreated with 50 nM MitoQ for 30 min before adding 1 nM GSK257815A. The effects of MitoQ, expressed as the percentage of autophagic cells (**d**) and percentage of cells with fragmented mitochondria (**e**), was assayed in cell cultures challenged with GSK2578215A for 12 h. 4-HNE fluorescence levels from confocal images were expressed as a.u. Values in the bar graphs are the mean ± S.E.M. of at least three independent experiments, each performed in triplicate. Statistical significance was determined by a two-tailed Student's *t*-test: $^{*}P < 0.05$ and $^{**}P < 0.01$

machinery of mitochondrial dynamics processes, including translocation of Drp-1 from the cytosol to the mitochondria. We evidenced the participation of autophagy as a cytoprotective response against the toxic effects induced by this inhibitor. The involvement of oxidative stress, which might act downstream of mitochondrial fission but upstream of autophagosome accumulation, is also revealed.

Our data demonstrated that LRRK2 inhibition activates autophagy. This conclusion was reached using two different approaches: a pharmacologic approach using GSK2578215A and LRRK2-IN-1 and molecularly using siRNA-induced knockdown of LRRK2 protein expression. Consistent with this, it has been shown that pharmacologic inhibition of LRRK2 kinase activity has an effect on autophagy.[45] Autophagy has been indicated to be a cellular machinery response against stress situations. Using GFP-LC3, we revealed how GSK2578215A significantly increased the autophagosome content in SH-SY5Y cells. Consistent with this, both under nutrient-rich (as we have used in this study), and starvation conditions, LRRK2 siRNA knockdown seemed to increase LC3-II levels.[4,46] Additionally, LRRK2-knockout mice displayed an increase in the number of autolysosomes structures.[47,48] On the other hand, earlier studies have shown that mutant LRRK2-induced toxicity is kinase-independent.[49,50] Moreover, it also has been shown that absence of LRRK2 causes bi-phasic (induction and depletion) alterations of the autophagy pathway,[48] and, conversely to our results, overexpression of wild-type and mutant LRRK2 is also associated with the accumulation of autophagosomes.[34,35] Of note, western blotting assays revealed that GSK2578215A significantly increased LC3 and p62 protein levels. Consistent with previous data,[35,45] the rise in p62 levels could be prevented by chemically blocking protein synthesis using CHX, suggesting that it may be due to an increase in *de novo* synthesis of p62 rather than a reduction in its degradation.

The use of GFP-LC3 allows us to quantify a possible upregulation of basal autophagy upon LRRK2 knockdown in a more meticulous way than immunoblot analysis,[51] and doing so, we ascertained the origin of the GSK2578215A increased number of autophagosomes within cells. Furthermore, our experiments performed with the mRFP-GFP-LC3 tandem reporter suggest that GSK2578215A inhibited autophagosome degradation.

In addition, our results allow us to order the cellular response to LRRK2 inhibition, and placed mitochondrial fission upstream of autophagic response. LRKK2 inhibition disrupts mitochondrial dynamics processes. After 6 h of treatment with GSK2578215A, activation of mitochondrial fission processes was evident. This result is very relevant, as abnormal fragmented mitochondria can no longer be properly distributed in the neuronal dendrites, and are unable to reach regions where ATP requirements are increased, leading to energy failure and synaptic damage.[52] Mitochondrial alterations are well documented and have been described in neurodegenerative disease models including 3-nitropropionic acid for Huntington disease,[53] β-amyloid peptide for Alzheimer's disease,[54] and 6-hydroxydopamine for PD.[24] Additionally, our data revealed that GSK2578215A-induced mitochondrial fission takes place through a process controlled by the fission-promoting protein Drp1. By using a chimeric protein fluorescent protein, we observed how Drp1 changes its localization from diffuse cytosolic to punctate mitochondrial localization. More importantly, GSK2578215A activates Drp1 translocation in a time-dependent manner, coinciding with the observed mitochondrial morphologic changes. Drp1 has critical roles in either physiologic or pathologic scenarios

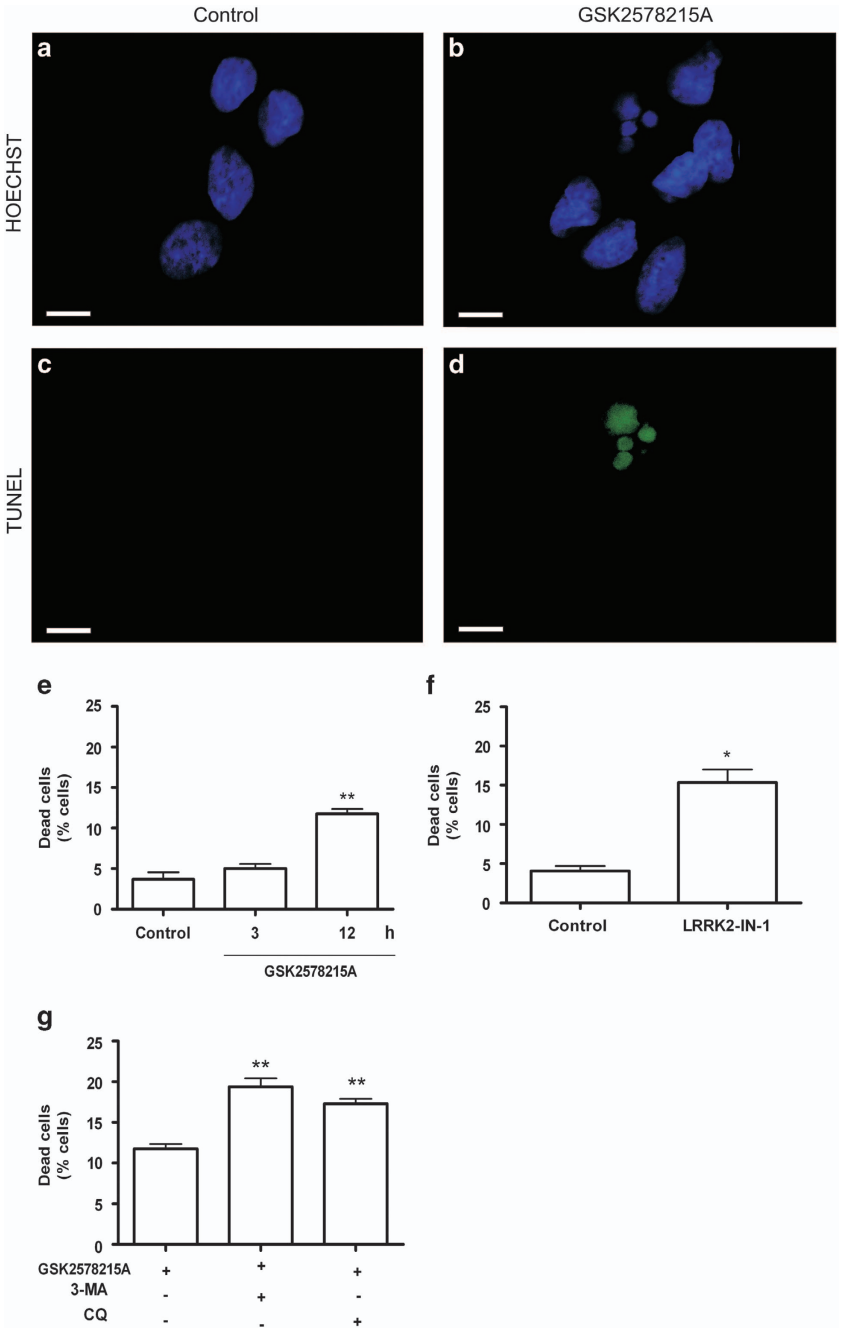

Figure 5 GSK2578215A induces apoptotical cell death in SH-SY5Y cultures. (**a** and **b**) Confocal images of SH-SY5Y chromatin stained with Hoechst 33342. Representative images of control cells (**a**) or incubated with 1 nM GSK2578215A for 24 h (**b**). In (**b**), note the presence of a cell with condensed or fragmented chromatin. (**c** and **d**) Representative confocal images of TUNEL analysis in SH-SY5Y cells, untreated (**c**) or challenged with 1 nM GSK57815A for 24 h (**d**). Scale bars, 10 μm. (**e**–**g**) Bar graphs showing the percentage of SH-SY5Y cells with death-like morphology at the indicated treatments: GSK57815A (1 nM) (**e**) and LRRK2-IN-1 (5 μM, 12 h) (**f**). (**e**) Before adding 1 nM GSK57815A, cell cultures were pretreated for 30 min with the autophagic disruptors 3-MA (5 mM) or CQ (50 μM) (**g**). Data shown are the mean ± S.E.M. of at least three independent experiments, each performed in triplicate. Statistical significance was determined by a two-tailed Student's *t*-test: $^{**}P<0.01$ and $^{***}P<0.001$

and is highly expressed in postmitotic neurons.[55] Interestingly, our study reveals how Drp1 functions as a key element. We inhibited Drp1 activity using mdivi-1. As described before, mdivi-1 attenuates mitochondrial division in yeast and mammalian cells by selectively inhibiting the mitochondrial division.[44] Consistent with this, previous work from our group and others showed the participation of this GTPase protein in neurodegenerative experimental models.[16,24,56] Upon blockage of the Drp1 function, we observed a decrease in the number of autophagosomes. In this line, inhibition of Drp1 has been proposed as a strategy for the treatment of PD.[57] Further evidence was obtained using a double transfection with two chimeric proteins to localize mitochondria and autophagosomes simultaneously. Doing so, we established that the distance between damaged mitochondria and the autophagosome decreased in a time-dependent manner.

Our results open the possibility that autophagy may have a cytoprotective role. GSK2578215A (1 nM) has a cytotoxic effect on SH-SY5Y cell cultures. Challenged cultures presented hallmarks of apoptosis such as fragmented chromatin and TUNEL-positive cells. Consistent with this, loss of LRRK2 markedly increases apoptotic cell death in LRRK2 $-/-$ mice[47] and further LRRK2 inhibitor drugs, although at higher concentrations than ours, results toxic in non-neuronal cells, including H4 and HEK293T cells.[45] Further, autophagy inhibition, by using either CQ or 3-MA, accelerated rather than abrogated GSK2578215A-induced cell death. In this regard, other studies have suggested a role for basal levels of autophagy in neuronal protection, and this is particularly important for the central nervous system. A prosurvival autophagic response is essential for cell survival under metabolic stress (for review a see Mizushima *et al.*[58]). In fact, genetic inactivation of autophagy causes neurodegeneration.[59,60] Interventions aimed at enhancing chaperone-mediated autophagy activity in PD have been proposed;[33] however, the precise mechanisms whereby disrupted mitochondria regulate autophagy remain unknown.

Consistent with previous observations,[61] our data support a significant role for ROS. First, we immunolocalized 4-HNE protein adducts, a hallmark of oxidative stress, in GSK2578215A-challenged cell cultures. In this regard, levels of protein carbonyls were markedly increased in the kidneys of *LRRK2* $-/-$ mice[47] and 4-HNE-modified proteins are shown to be accumulated in the post-mortem brain of PD patients.[62] Second, the use of a specific mitochondrial-addressed scavenger drug, MitoQ, allowed us to show that ROS released by mitochondria are involved in LRRK2-activated pathways. MitoQ makes use of the TPP ion to accumulate into the organelle by virtue of the mitochondrial membrane potential gradient, and then blocks ROS release. Recently, we have shown how MitoQ is able to prevent mitochondrial morphology alterations induced by subtoxic concentrations of the parkinsonian toxin 6-hydroxydopamine.[23] Taken together, the results presented here support the hypothesis that mitochondrial dysfunction causes an increase in the amount of mitochondrial-generated ROS, which in turns leads to oxidative stress and activation of the autophagy response pathway. As MitoQ failed to block GSK2578215A-induced mitochondrial fission, it is conceivable that oxidative stress or derived lipid peroxidation products may intervene in later steps.

In summary, our data show how LRRK2 inhibition activates a cellular response where autophagy results in cytoprotection downstream of a disruption of the mitochondrial dynamics balance via a Drp1-dependent process. Our study suggests that drugs that modulate the functions of Drp1 or mitochondrial-ROS may represent new opportunities to slow down neurodegeneration linked to PD.

Materials and Methods

Reagents and plasmids. DMEM-F12 (Dulbecco's modified Eagle's medium), penicillin–streptomycin, gentamicin and fetal bovine serum (FBS) were purchased from Gibco-Invitrogen (Carlsbad, CA, USA). GSK 2578215A and LRRK2-IN-1 were purchased from Tocris Bioscience (Minneapolis, MN, USA). Stealth RNAi duplexes were purchased from Life Technologies (Carlsbad, CA, USA). BCA protein assay was from Pierce (Rockford, IL, USA). The pDsRed2-mito vector was provided by Clontech (BD Biosciences, San Jose, CA, USA), GFP-LC3 was provided by Dr. JM Fuentes (Universidad de Extremadura, Badajoz, Spain), Drp1-GFP was provided by T Wilson and Dr. S Strack (Department of Pharmacology, University of Iowa Carver College of Medicine, Iowa City, IA, USA) and mRFP-GFP-LC3 was provided by Dr. E Kneck (Laboratory of Cellular Biology, Centro de Investigación Príncipe Felipe, Valencia, Spain). Anti-4 hydroxynonenal and LRRK2 antibodies were purchased from Abcam (Cambridge, UK); anti-p62 from BD (San Jose, CA, USA) and Alexa Fluor 488 were from Molecular Probes (Carlsbad, CA, USA), Invitrogen (Carlsbad, CA, USA); and anti-acetylated tubulin was from Sigma-Aldrich (St. Louis, MO, USA). The TUNEL method (MEBSTAIN Apoptosis Kit) was purchased from MBL (Carlsbad, CA, USA). Mdivi-1 was purchased from Sigma-Aldrich.

Cell culture and drug treatment procedures. SH-SY5Y cell lines were obtained from American Type Culture Collection (ATCC, Manassas, VA, USA). Cells cultures were grown in DMEM-F12 supplemented with 2 mM L-glutamine, 20 U/ml penicillin–streptomycin, 5 mg/ml gentamicin and 15% (v/v) FBS. Cells were grown in a humidified cell incubator at 37 °C under a 5% CO_2 atmosphere. GSK 2578215A was added to the culture medium at final concentrations of 1 nM. Pretreatment with MitoQ (50 nM), 3-MA (5 mM), CQ (50 μM) or Mdivi-1 (10 μM) was added 30 min before treatment.

Cell viability. Cell viability was analyzed by phase-contrast microscopy. Healthy cells were identified as having smooth, phase-bright cell bodies and intact neurites. Cells exhibiting a rough appearance with irregular-shaped cell bodies, blebs and vacuoles, followed by cell shrinkage, and loss of phase brightness, were considered to be damaged. We performed the experiments using a 'blind' counter. A total of 200–400 cells were examined in three to five randomized subfields of the coverslips. Results are expressed as the percentage of cell survival as compared with untreated cells. Each condition was represented by three coverslips. All the experiments were performed in quadruplicate.

Chromatin state. SH-SY5Y cells were spotted on poly-D-lysine-coated glass slides. After treatment, the glass slides were rinsed three times with PBS and then incubated with 0.5 μg/ml of Hoechst 33342 (Molecular Probes Inc., Eugene, OR, USA) for 5 min at room temperature. After two rinses with PBS, chromatin staining was analyzed using a fluorescent microscope. Uniformly stained nuclei were scored as healthy, viable cells. Condensed or fragmented nuclei were scored as apoptotic.

TUNNEL. TUNEL staining was performed using TDT (MBL) according to the suggestions of the manufacturer. Briefly, cells were fixed with 4% paraformaldehyde (PFA) and then incubated with a mixture of TUNNEL buffer (TdT buffer) and FITC-dUTP solution for 60 min. TUNEL staining was monitored under confocal microscope.

Transfections. Twenty-four hours before transfection, cells were plated at a density of 5.3×10^4 cells per cm^2 on IDIBI-coated dishes. Transfection was achieved using Lipofectamine reagent (Invitrogen) according to the manufacturer's protocol. Cells were transfected with the following plasmids encoding pDsRed2, GFP-Drp1, GFP-LC3 and mRFP-GFP-LC3. After 4 h incubation, the transfection mixture was removed and replaced with fresh complete medium. The experiments were performed 24 h after transfection to allow protein expression. To knockdown LRRK2, SH-SY5Y cells were transfected with Lipofectamine 2000 (Invitrogen) using LRRK2 Stealth RNAi duplexes (Invitrogen), as described by the manufacturer. For autophagy and mitochondrial analysis, SH-SY5Y cells were co-transfected with plasmid encoding pDsRed2 or GFP-LC3 and Stealth RNAi duplexes as described by the manufacturer.

Mitochondrial morphology. Cells were transfected with pDsRed2-mito, which leads to the expression of fluorescent DsRed2 in the mitochondria, thereby labeling the organelles. The transfected cells are then subjected to experimental treatments to evaluate mitochondrial morphology by fluorescence microscopy. For quantification, the percentage of cells with abnormal mitochondrial morphologies was determined and taken as a measure of the proportion of cells with fragmented mitochondria. Most of the cells had either fragmented or filamentous mitochondria, whereas a small percentage of the cells contained both fragmented and filamentous mitochondria. In case of the latter, the mitochondrial morphology was classified according to the majority ($>70\%$) of the mitochondria. The monitoring of the mitochondrial morphology was performed by two 'blind' independent examiners on three different cultures. Micrographs were processed with Huygens

Deconvolution Software (Scientific Volume Imaging, Hilversun, The Netherlands) and Adobe Photoshop.

Autophagic cells. Cells were transfected with GFP-LC3, which leads to the expression of fluorescent LC3, the universal marker protein of autophagic structures in mammalian and yeast cultured cells. The transfected cells are then subjected to experimental treatments to evaluate the percentage of autophagic cells. Non-treated cells showed diffuse cytosolic LC3 distribution, whereas the appearance of LC3-positive punctate is indicative of the induction of autophagy. For quantification, all cells with more than six autophagosomes per cell are considered as autophagic cells.

Autophagic flux. The assays were conducted with confocal microscopy on an SH-SY5Y cell line that was transiently transfected with GFP-LC3 treated with GSK2578215A in the presence or absence of 50 μM CQ, which clamps the degradation. Briefly and according to Klionsky *et al.*, [63] we analyzed autophagic flux using GFP-LC3 fluorescence by adding lysosomal protease inhibitor (CQ) to cells expressing GFP-LC3, and monitoring changes in the number of dots. Autophagosome synthesis was defined as the number of GFP-LC3 dots per cell in cell cultures treated with CQ. Thus, the synthesis measured the increase of GFP-LC3 dots or autophagosomes, stimulated by GSK 2578215A in the presence of CQ. A positive value indicates a net increase in these parameters, thus suggesting a promotion of autophagy process.

Western blotting. SH-SY5Y cell cultures were washed with ice-cold PBS two times and then collected by mechanical scraping with 1 ml of PBS per tissue culture dish. The suspension was centrifuged at 12 000–14 000 r.p.m. for 5 min. The supernatant was discarded, and the pellet was raised in 150 μl of sample buffer. The protein from each condition was quantified spectrophotometrically (Micro BCA Protein Reagent Kit; Pierce), and an equal amount of protein (30 μg) was loaded onto 10% SDS-PAGE gels. After electrophoresis, proteins were transferred to polyvinylidene difluoride membranes (Immobilon; Millipore Corporation, Billerica, MA, USA). Nonspecific protein binding was blocked with Blotto (4% (w/v) nonfat dried milk, 4% bovine serum albumin (Sigma), and 0.1% Tween-20 (Sigma)) in PBS for 1 h. The membranes were incubated with specific antibodies. After washing with Blotto, the membranes were incubated with peroxidase-labeled anti-rabbit or anti-mouse secondary antibodies (Promega) in Blotto. The signal was detected using an Enhanced Chemiluminescence Detection Kit (GE Healthcare, Little Chalfont, Buckinghamshire, UK). Band intensity was estimated densitometrically on a GS-800 calibrated densitometer (Bio-Rad Quantity One; Bio-Rad, Hercules, CA, USA).

4-HNE immunofluorescence. For assessment of immunofluorescence, SH-SY5Y cells were plated on poly-L-lysine-coated glass slides. Cells were fixed with 4% PFA in PBS 10 min at 37 °C and washed two times with PBS. After permeabilization, cells were incubated overnight with anti-4 hydroxynonenal (4HNEJ-2; Abcam) at 4 °C. Then, cells were incubated with fluorescent-conjugated secondary antibodies Alexa Fluor 488 (Molecular Probes, Invitrogen) for 1 h at RT. 4-HNE expression was quantified by measuring optical density with ImageJ software (National Institute of Mental Health, Bethesda, MD, USA). After quantification, the density of staining was calculated by dividing the pixel count by the cell number to get pixels per cell.

Statistical analysis. Data shown are means ± S.E.M. Statistical significance was determined by a two-tailed Student's *t*-test. The statistical significance was set at $P < 0.05$.

Conflict of Interest

The authors declare no conflict of interest.

Acknowledgements. This work is dedicated in the loving memory of the father of Joaquin Jordan. We thank Carlos Garrido for technical help, and T Wilson, Dr. S Strack and Dr. JHM Prehn for providing the vectors. This work was supported by 'Incorporación de grupos emergentes' FIS CARLOS III (EMER07/023), FIS-FEDER (PI080693; PI-2008/21) (to MFG) and UCV grants (UCV 2012-011-001; 2013-168-001) (to JRB). SS is a predoctoral fellow of 'Universidad Católica de Valencia' (UCV).

1. Gilks WP, Abou-Sleiman PM, Gandhi S, Jain S, Singleton A, Lees AJ *et al.* A common LRRK2 mutation in idiopathic Parkinson's disease. *Lancet* 2005; **365**: 415–416.
2. Lesage S, Janin S, Lohmann E, Leutenegger AL, Leclere L, Viallet F *et al.* LRRK2 exon 41 mutations in sporadic Parkinson disease in Europeans. *Arch Neurol* 2007; **64**: 425–430.
3. Bardien S, Lesage S, Brice A, Carr J. Genetic characteristics of leucine-rich repeat kinase 2 (LRRK2) associated Parkinson's disease. *Parkinsonism Relat Disord* 2011; **17**: 501–508.
4. Alegre-Abarrategui J, Christian H, Lufino MM, Mutihac R, Venda LL, Ansorge O *et al.* LRRK2 regulates autophagic activity and localizes to specific membrane microdomains in a novel human genomic reporter cellular model. *Hum Mol Genet* 2009; **18**: 4022–4034.
5. Gandhi PN, Wang X, Zhu X, Chen SG, Wilson-Delfosse AL. The Roc domain of leucine-rich repeat kinase 2 is sufficient for interaction with microtubules. *J Neurosci Res* 2008; **86**: 1711–1720.
6. Gillardon F. Leucine-rich repeat kinase 2 phosphorylates brain tubulin-beta isoforms and modulates microtubule stability–a point of convergence in parkinsonian neurodegeneration? *J Neurochem* 2009; **110**: 1514–1522.
7. Valiron O, Caudron N, Job D. Microtubule dynamics. *Cell Mol Life Sci* 2001; **58**: 2069–2084.
8. Guerreiro PS, Huang Y, Gysbers A, Cheng D, Gai WP, Outeiro TF *et al.* LRRK2 interactions with alpha-synuclein in Parkinson's disease brains and in cell models. *J Mol Med (Berl)* 2013; **91**: 513–522.
9. Meixner A, Boldt K, Van Troys M, Askenazi M, Gloeckner CJ, Bauer M *et al.* A QUICK screen for Lrrk2 interaction partners – leucine-rich repeat kinase 2 is involved in actin cytoskeleton dynamics. *Mol Cell Proteom* 2011; **10**: M110 001172.
10. West AB, Moore DJ, Biskup S, Bugayenko A, Smith WW, Ross CA *et al.* Parkinson's disease-associated mutations in leucine-rich repeat kinase 2 augment kinase activity. *Proc Natl Acad Sci USA* 2005; **102**: 16842–16847.
11. Greggio E, Jain S, Kingsbury A, Bandopadhyay R, Lewis P, Kaganovich A *et al.* Kinase activity is required for the toxic effects of mutant LRRK2/dardarin. *Neurobiol Dis* 2006; **23**: 329–341.
12. Smith WW, Pei Z, Jiang H, Dawson VL, Dawson TM, Ross CA. Kinase activity of mutant LRRK2 mediates neuronal toxicity. *Nat Neurosci* 2006; **9**: 1231–1233.
13. Tong Y, Shen J. Alpha-synuclein and LRRK2: partners in crime. *Neuron* 2009; **64**: 771–773.
14. Lin X, Parisiadou L, Gu XL, Wang L, Shim H, Sun L *et al.* Leucine-rich repeat kinase 2 regulates the progression of neuropathology induced by Parkinson's-disease-related mutant alpha-synuclein. *Neuron* 2009; **64**: 807–827.
15. Wszolek ZK, Pfeiffer RF, Tsuboi Y, Uitti RJ, McComb RD, Stoessl AJ *et al.* Autosomal dominant parkinsonism associated with variable synuclein and tau pathology. *Neurology* 2004; **62**: 1619–1622.
16. Gomez-Lazaro M, Bonekamp NA, Galindo MF, Jordan J, Schrader M. 6-Hydroxydopamine (6-OHDA) induces Drp1-dependent mitochondrial fragmentation in SH-SY5Y cells. *Free Radic Biol Med* 2008; **44**: 1960–1969.
17. Gomez-Lazaro M, Galindo MF, Concannon CG, Segura MF, Fernandez-Gomez FJ, Llecha N *et al.* 6-Hydroxydopamine activates the mitochondrial apoptosis pathway through p38 MAPK-mediated, p53-independent activation of Bax and PUMA. *J Neurochem* 2008; **104**: 1599–1612.
18. Exner N, Lutz AK, Haass C, Winklhofer KF. Mitochondrial dysfunction in Parkinson's disease: molecular mechanisms and pathophysiological consequences. *EMBO J* 2012; **31**: 3038–3062.
19. Iaccarino C, Crosio C, Vitale C, Sanna G, Carri MT, Barone P. Apoptotic mechanisms in mutant LRRK2-mediated cell death. *Hum Mol Genet* 2007; **16**: 1319–1326.
20. Youle RJ, van der Bliek AM. Mitochondrial fission, fusion, and stress. *Science* 2012; **337**: 1062–1065.
21. Youle RJ, Karbowski M. Mitochondrial fission in apoptosis. *Nat Rev Mol Cell Biol* 2005; **6**: 657–663.
22. Galindo MF, Solesio ME, Atienzar-Aroca S, Zamora MJ, Jordan Bueso J. Mitochondrial dynamics and mitophagy in the 6-hydroxydopamine preclinical model of Parkinson's disease. *Parkinsons Dis* 2012; **2012**: 131058.
23. Solesio ME, Prime TA, Logan A, Murphy MP, Del Mar Arroyo-Jimenez M, Jordan J *et al.* The mitochondria-targeted anti-oxidant MitoQ reduces aspects of mitochondrial fission in the 6-OHDA cell model of Parkinson's disease. *Biochim Biophys Acta* 2013; **1832**: 174–182.
24. Solesio ME, Saez-Atienzar S, Jordan J, Galindo MF. Characterization of mitophagy in the 6-hydoxydopamine Parkinson's disease model. *Toxicol Sci* 2012; **129**: 411–420.
25. Schon EA, Przedborski S. Mitochondria: the next (neurode)generation. *Neuron* 2011; **70**: 1033–1053.
26. Labrousse AM, Zappaterra MD, Rube DA, van der Bliek AMC. elegans dynamin-related protein DRP-1 controls severing of the mitochondrial outer membrane. *Mol Cell* 1999; **4**: 815–826.
27. Legesse-Miller A, Massol RH, Kirchhausen T. Constriction and Dnm1p recruitment are distinct processes in mitochondrial fission. *Mol Biol Cell* 2003; **14**: 1953–1963.
28. Stafa K, Tsika E, Moser R, Musso A, Glauser L, Jones A *et al.* Functional interaction of Parkinson's disease-associated LRRK2 with members of the dynamin GTPase superfamily. *Hum Mol Genet* 2013; **23**: 2055–2077.
29. Sridhar S, Botbol Y, Macian F, Cuervo AM. Autophagy and disease: always two sides to a problem. *J Pathol* 2012; **226**: 255–273.

30. Loos B, Engelbrecht AM, Lockshin RA, Klionsky DJ, Zakeri Z. The variability of autophagy and cell death susceptibility: Unanswered questions. *Autophagy* 2013; **9**: 1270–1285.
31. Kabeya Y, Mizushima N, Ueno T, Yamamoto A, Kirisako T, Noda T *et al.* LC3, a mammalian homologue of yeast Apg8p, is localized in autophagosome membranes after processing. *EMBO J* 2000; **19**: 5720–5728.
32. Yamamoto H, Kakuta S, Watanabe TM, Kitamura A, Sekito T, Kondo-Kakuta C *et al.* Atg9 vesicles are an important membrane source during early steps of autophagosome formation. *J Cell Biol* 2012; **198**: 219–233.
33. Orenstein SJ, Kuo SH, Tasset I, Arias E, Koga H, Fernandez-Carasa I *et al.* Interplay of LRRK2 with chaperone-mediated autophagy. *Nat Neurosci* 2013; **16**: 394–406.
34. Gomez-Suaga P, Churchill GC, Patel S, Hilfiker S. A link between LRRK2, autophagy and NAADP-mediated endolysosomal calcium signalling. *Biochem Soc Trans* 2012; **40**: 1140–1146.
35. Gomez-Suaga P, Hilfiker S. LRRK2 as a modulator of lysosomal calcium homeostasis with downstream effects on autophagy. *Autophagy* 2012; **8**: 692–693.
36. Biskup S, Moore DJ, Celsi F, Higashi S, West AB, Andrabi SA *et al.* Localization of LRRK2 to membranous and vesicular structures in mammalian brain. *Ann Neurol* 2006; **60**: 557–569.
37. Yoritaka A, Hattori N, Uchida K, Tanaka M, Stadtman ER, Mizuno Y. Immunohistochemical detection of 4-hydroxynonenal protein adducts in Parkinson disease. *Proc Natl Acad Sci USA* 1996; **93**: 2696–2701.
38. Hattori N, Wanga M, Taka H, Fujimura T, Yoritaka A, Kubo S *et al.* Toxic effects of dopamine metabolism in Parkinson's disease. *Parkinsonism Relat Disord* 2009; **15**(Suppl 1): S35–S38.
39. Kramer T, Lo Monte F, Goring S, Okala Amombo GM, Schmidt B. Small molecule kinase inhibitors for LRRK2 and their application to Parkinson's Disease Models. *ACS Chem Neurosci* 2012; **3**: 151–160.
40. Reith AD, Bamborough P, Jandu K, Andreotti D, Mensah L, Dossang P *et al.* GSK2578215A; a potent and highly selective 2-arylmethyloxy-5-substitutent-N-arylbenzamide LRRK2 kinase inhibitor. *Bioorg Med Chem Lett* 2012; **22**: 5625–5629.
41. Law BM, Spain VA, Leinster VH, Chia R, Beilina A, Cho HJ *et al.* A direct interaction between leucine-rich repeat kinase 2 and specific beta-tubulin isoforms regulates tubulin acetylation. *J Biol Chem* 2014; **289**: 895–908.
42. Parisiadou L, Xie C, Cho HJ, Lin X, Gu XL, Long CX *et al.* Phosphorylation of ezrin/radixin/moesin proteins by LRRK2 promotes the rearrangement of actin cytoskeleton in neuronal morphogenesis. *J Neurosci* 2009; **29**: 13971–13980.
43. Kimura S, Noda T, Yoshimori T. Dissection of the autophagosome maturation process by a novel reporter protein, tandem fluorescent-tagged LC3. *Autophagy* 2007; **3**: 452–460.
44. Cassidy-Stone A, Chipuk JE, Ingerman E, Song C, Yoo C, Kuwana T *et al.* Chemical inhibition of the mitochondrial division dynamin reveals its role in Bax/Bak-dependent mitochondrial outer membrane permeabilization. *Dev Cell* 2008; **14**: 193–204.
45. Manzoni C, Mamais A, Dihanich S, Abeti R, Soutar MP, Plun-Favreau H *et al.* Inhibition of LRRK2 kinase activity stimulates macroautophagy. *Biochim Biophys Acta* 2013; **1833**: 2900–2910.
46. Higashi S, Moore DJ, Yamamoto R, Minegishi M, Sato K, Togo T *et al.* Abnormal localization of leucine-rich repeat kinase 2 to the endosomal-lysosomal compartment in lewy body disease. *J Neuropathol Exp Neurol* 2009; **68**: 994–1005.
47. Tong Y, Yamaguchi H, Giaime E, Boyle S, Kopan R, Kelleher RJ 3rd *et al.* Loss of leucine-rich repeat kinase 2 causes impairment of protein degradation pathways, accumulation of alpha-synuclein, and apoptotic cell death in aged mice. *Proc Natl Acad Sci USA* 2010; **107**: 9879–9884.
48. Tong Y, Giaime E, Yamaguchi H, Ichimura T, Liu Y, Si H *et al.* Loss of leucine-rich repeat kinase 2 causes age-dependent bi-phasic alterations of the autophagy pathway. *Mol Neurodegener* 2012; **7**: 2.
49. Skibinski G, Nakamura K, Cookson MR, Finkbeiner S. Mutant LRRK2 toxicity in neurons depends on LRRK2 levels and synuclein but not kinase activity or inclusion bodies. *J Neurosci* 2014; **34**: 418–433.
50. Wang X, Yan MH, Fujioka H, Liu J, Wilson-Delfosse A, Chen SG *et al.* LRRK2 regulates mitochondrial dynamics and function through direct interaction with DLP1. *Hum Mol Genet* 2012; **21**: 1931–1944.
51. Ding WX, Li M, Chen X, Ni HM, Lin CW, Gao W *et al.* Autophagy reduces acute ethanol-induced hepatotoxicity and steatosis in mice. *Gastroenterology* 2010; **139**: 1740–1752.
52. Nakamura T, Lipton SA. Redox modulation by S-nitrosylation contributes to protein misfolding, mitochondrial dynamics, and neuronal synaptic damage in neurodegenerative diseases. *Cell Death Differ* 2011; **18**: 1478–1486.
53. Solesio ME, Saez-Atienzar S, Jordan J, Galindo MF. 3-Nitropropionic acid induces autophagy by forming mitochondrial permeability transition pores rather than activating the mitochondrial fission pathway. *Br J Pharmacol* 2013; **168**: 63–75.
54. Cho DH, Nakamura T, Fang J, Cieplak P, Godzik A, Gu Z *et al.* S-nitrosylation of Drp1 mediates beta-amyloid-related mitochondrial fission and neuronal injury. *Science* 2009; **324**: 102–105.
55. Cho B, Choi SY, Cho HM, Kim HJ, Sun W. Physiological and pathological significance of dynamin-related protein 1 (Drp1)-dependent mitochondrial fission in the nervous system. *Exp Neurobiol* 2013; **22**: 149–157.
56. Haun F, Nakamura T, Shiu AD, Cho DH, Tsunemi T, Holland EA *et al.* S-nitrosylation of dynamin-related protein 1 mediates mutant huntingtin-induced mitochondrial fragmentation and neuronal injury in Huntington's disease. *Antioxid Redox Signal* 2013; **19**: 1173–1184.
57. Su YC, Qi X. Inhibition of excessive mitochondrial fission reduced aberrant autophagy and neuronal damage caused by LRRK2 G2019S mutation. *Hum Mol Genet* 2013; **22**: 4545–4561.
58. Mizushima N, Levine B, Cuervo AM, Klionsky DJ. Autophagy fights disease through cellular self-digestion. *Nature* 2008; **451**: 1069–1075.
59. Hara T, Nakamura K, Matsui M, Yamamoto A, Nakahara Y, Suzuki-Migishima R *et al.* Suppression of basal autophagy in neural cells causes neurodegenerative disease in mice. *Nature* 2006; **441**: 885–889.
60. Komatsu M, Waguri S, Chiba T, Murata S, Iwata J, Tanida I *et al.* Loss of autophagy in the central nervous system causes neurodegeneration in mice. *Nature* 2006; **441**: 880–884.
61. Mizushima N, Komatsu M. Autophagy: renovation of cells and tissues. *Cell* 2011; **147**: 728–741.
62. Hattoria N, Wanga M, Taka H, Fujimura T, Yoritaka A, Kubo S *et al.* Toxic effects of dopamine metabolism in Parkinson's disease. *Parkinsonism Relat Disord* 2009; **15**(Suppl 1): S35–S38.
63. Klionsky DJ, Abdalla FC, Abeliovich H, Abraham RT, Acevedo-Arozena A, Adeli K *et al.* Guidelines for the use and interpretation of assays for monitoring autophagy. *Autophagy* 2012; **8**: 445–544.

Supplementary Information accompanies this paper on Cell Death and Disease website (http://www.nature.com/cddis)